https://doi.org/10.26599/SES.2026.9590027

Research Article

Numerical simulation of hydrogen leakage and explosion characteristics in hydrogen fuel cell buses under different window-opening conditions and wind directions

Qifeng Li, Tianmin Yu, Chenghao Ge, Hao Diao, Jie Chen (✉)

Henan Polytechnic University, Henan, China

✉ chenj1996@hpu.edu.cn

Received: June 29, 2026; Revised: August 5, 2026; Accepted: August 25, 2026

Abstract: With the large-scale deployment of hydrogen fuel cell buses, operational safety concerns have become increasingly prominent, particularly the risks associated with hydrogen leakage and subsequent explosion, which warrant thorough evaluation. Using the Computational Fluid Dynamics (CFD) simulation software, a three-dimensional physical model was constructed based on a specific hydrogen fuel cell bus prototype to systematically investigate the leakage and dispersion characteristics of hydrogen within the cabin, as well as the associated combustion and explosion hazards, under varying numbers of open windows and wind directions. The results indicate that hydrogen leakage in a confined space exhibits pronounced vertical concentration stratification. The number of open windows significantly influences the distribution of the hydrogen concentration field within the passenger cabin. However, when the number of open windows is held constant, the impact of different window opening locations on the hydrogen volume fraction at a given monitoring point is relatively minor. Furthermore, when the explosion overpressure generated by the ignition of the leaked hydrogen exceeds the ultimate load-bearing capacity of the window glass, the glass fractures, thereby achieving pressure relief. A comprehensive assessment reveals that the high-temperature thermal hazards induced by hydrogen combustion are significantly greater than the blast overpressure hazards in confined-space combustion and explosion scenarios.

Keywords: Hydrogen fuel cell bus; Hydrogen leakage; Hydrogen combustion and explosion; CFD numerical simulation

1 Introduction

Driven by the global energy transition and the "Dual Carbon" strategic goals, hydrogen energy is increasingly emerging as a research hotspot in the new energy sector, owing to its advantages of being clean and emission-free, possessing a high heating value, featuring abundant sources, and enabling high energy conversion efficiency. The application of hydrogen fuel cell technology in the transportation sector can effectively mitigate energyrelated pollution and carbon emissions within this domain (Kulikovsky, 2019; Chen et al., 2020). However, as a highly flammable and explosive gas, hydrogen exhibits distinct physicochemical properties, including a high diffusion rate, low minimum ignition energy, wide flammability limits (4%–75% of volume), and rapid flame propagation speed, which pose significant challenges to safety management and control throughout its production, storage, transportation, and utilization stages (Moradi and Groth, 2019; Najjar, 2013; Guo et al., 2024). A combustion and explosion incident could result in catastrophic consequences, particularly within high-occupancy hydrogen fuel cell buses (Yang et al., 2021). Furthermore, complex road conditions during bus operation, external environmental factors, and the hydrogen embrittlement of hydrogen storage materials may all induce the risk of hydrogen leakage. Ensuring the safe application of hydrogen energy in the public transportation sector has emerged as a critical challenge constraining its large-scale deployment (Khalil, 2018; Roes and Patel, 2011).

As hydrogen applications continue to expand, researchers globally have conducted extensive investigations into hydrogen safety across various application scenarios. These studies can be broadly classified into two main categories, including experimental research and numerical simulation. Among these, experimental studies primarily focus on analyzing hydrogen leakage and explosion characteristics, as well as validating associated theoretical models (Tanaka et al., 2007; Mogi et al., 2008; Xiao et al., 2018; Lu et al., 2024). In numerical simulation studies, existing research primarily focuses on the assessment and analysis of hydrogen leakage and its associated combustion and explosion risks across various scenarios. Lucas M et al. (2021) conducted numerical simulations of the vented explosion process of homogeneous and inhomogeneous hydrogen clouds within a 20-foot container using the FLACS-Hydrogen software. The computational results were compared with experimental data from the HySEA project, with a primary focus on validating the computational accuracy of the modified Flacs3 solver in simulating stratified gas explosions. Zhao (2021) conducted numerical simulations of the leakage and explosion processes of fuel cell vehicles in underground garages using the FLACS software. Integrating numerical simulations with injury models enables a more flexible assessment of the potential hazards to humans from accidents in the environments. Vyazmina and Jallais (2016) validated the performance of the FLACS software in simulating hydrogen vented explosions. The results indicate that the software can yield reasonably accurate results when modeling vented explosion processes in large confined spaces. Li et al. (2019) conducted numerical simulations of the gas explosion process in the natural gas compartment of a utility tunnel using the FLACS software, revealing the flame propagation mechanism and the distribution characteristics of explosion overpressure. Xu et al. (2024) employed the FLUENT software to conduct numerical simulations of hydrogen leakage and explosion processes in hydrogen fuel cell buses under various operating conditions. The results indicate that, in the event of an accidental hydrogen explosion, the hazard posed by high-temperature thermal radiation significantly exceeds that from shock wave overpressure. Cui et al. (2023) employed the FLACS software to conduct fire hazard analysis and numerical simulations of hydrogen leakage and explosion in hydrogen fuel cell vehicles. The results indicate that the fire hazard associated with vertical hydrogen leakage exceeds that of horizontal leakage, with the highest risk observed under the vertically downward leakage scenario. Mao et al. (2021) conducted numerical simulations of hydrogen leakage and explosion processes in hydrogen fuel cell vessels. The resulting high-temperature and high-pressure distribution characteristics can provide a scientific basis for optimizing safety design, enhancing risk management, and formulating personnel evacuation plans, thereby effectively reducing accident losses. Malakhov et al. (2020) employed CFD to investigate the spatial distribution patterns of hydrogen clouds following leakage in semi-enclosed ventilated facilities under various combinations of release pressure and leak orifice diameter. The findings of this study can provide a reference for hydrogen safety assessments in similar semi-enclosed structures.

Previous studies on hydrogen leakage and explosion hazards in hydrogen fuel cell buses have primarily focused on either the leakage and diffusion behavior of hydrogen or its explosion characteristics in isolation, while few studies have investigated the entire process from leakage and dispersion to subsequent ignition as an integrated whole. Moreover, many existing studies have neglected the effects of external factors, such as ambient wind speed, wind direction, and the number and location of open passenger windows, on the hydrogen cloud behavior, or have only considered ignition under a single operating condition. This paper employs CFD to analyze the combustion and explosion risks associated with hydrogen leaks in fuel cell buses. The simulation considers how window positioning, quantity, and wind direction affect the hydrogen cloud during leakage events, while ignition of the leaked gas cloud simulates actual explosion scenarios, thereby it more accurately reflects the actual situation.

2 Model formulation

2.1 Geometric model

A computational model was developed based on a commercially available hydrogen fuel cell bus, with appropriate simplifications applied according to the research focus. The vehicle is equipped with six hydrogen storage cylinders, each with a capacity of 140 L, has dimensions of 10.5 m × 2.5 m × 3.0 m, and a rated passenger capacity of 69. The corresponding geometric model in CFD simulation software is shown in Fig. 1. Given the complex internal piping layout and the highly variable operating conditions of hydrogen fuel cell buses, the hydrogen supply system poses a significant leakage risk. Consequently, the leakage source is positioned at the center of the bus undercarriage, with 100% pure hydrogen as the leakage medium. The leak orifice dimensions are set to 0.1 m × 0.1 m (Hou, 2023), and the mass leakage rate is 20 g/s (Xu et al., 2024).

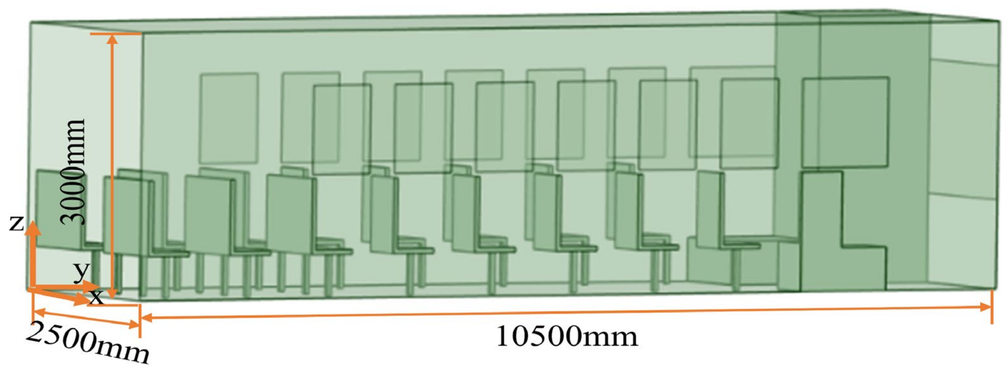

Fig. 1 Geometric model of a hydrogen fuel cell bus

2.2 Mathematical model

The finite volume method is employed to solve the compressible conservation equations on a three-dimensional Cartesian grid. This system of equations comprises the conservation equations for mass, momentum, enthalpy, and species mass fractions, and is closed using the ideal gas equation of state.

The general form of the conservation equations can be expressed as follows.

$$\frac{\partial}{\partial t}(\rho\phi)+\frac{\partial}{\partial x_j}(\rho u_j\phi)-\frac{\partial}{\partial x_j}\left(\rho\Gamma_\phi\frac{\partial}{\partial x_j}(\phi)\right)=S_\phi \qquad \text{Eq.1}$$

$$\Gamma_\phi=\frac{\mu_{eff}}{\sigma_\phi} \qquad \text{Eq.2}$$

$$\mu_{eff}=\mu+\rho C_\mu\frac{k^2}{\varepsilon} \qquad \text{Eq.3}$$

Where ϕ denotes the general variable to be solved, ρ is the density, u is the dynamic viscosity, μ_{eff} is the effective viscosity, σ_ϕ is the turbulent Prandtl-Schmidt number, S_ϕ is the source term, k is the turbulent kinetic energy, and ε is the turbulent dissipation rate.

2.2.1 Governing equations

The fundamental governing equations employed to solve compressible fluid flow comprise the mass conservation equation, momentum conservation equation, energy conservation equation, fuel mass fraction transport equation, and mixture fraction transport equation.

Mass conservation equation.

$$\frac{\partial}{\partial t}(\beta_v\rho)+\frac{\partial}{\partial x_j}(\beta_j\rho u_j)=\frac{\dot{m}}{V} \qquad \text{Eq.4}$$

Where β_v denotes the volumetric porosity, and β_j represents the area porosity in the j-direction.

Momentum conservation equation.

$$\frac{\partial}{\partial t}(\beta_v \rho u_i)+\frac{\partial}{\partial x_j}\left(\beta_j \rho u_i u_j\right)=-\beta_v \frac{\partial p}{\partial x_i}+\frac{\partial}{\partial x_j}\left(\beta_j \sigma_{ij}\right)+F_{o,i}+F_{w,i}+\beta_v\left(\rho-\rho_0\right)g_i \quad \text{Eq.5}$$

Where σ_{ij} denotes the stress tensor, $F_{o,i}$ represents the subgrid flow resistance, and $F_{w,i}$ denotes the wall-induced flow resistance.

Energy conservation equation.

$$\frac{\partial}{\partial t}(\beta_v \rho h)+\frac{\partial}{\partial x_j}(\beta_j \rho u_j h)=\frac{\partial}{\partial x_j}\left(\beta_j \frac{\mu_{\text{eff}}}{\sigma_h}\frac{\partial h}{\partial x_j}\right)+\beta_v \frac{Dp}{Dt}+\frac{\dot{Q}}{V} \quad \text{Eq.6}$$

In the formula, σ_h is the Prandtl–Schmidt enthalpy number, with a value of 0.7.

Fuel mass fraction transport equation.

$$\frac{\partial}{\partial t}\left(\beta_v \rho Y_{\text{fuel}}\right)+\frac{\partial}{\partial x_j}\left(\beta_j \rho u_j Y_{\text{fuel}}\right)=\frac{\partial}{\partial x_j}\left(\beta_j \frac{\mu_{\text{eff}}}{\sigma_{\text{fuel}}}\frac{\partial Y_{\text{fuel}}}{\partial x_j}\right)+R_{\text{fuel}} \quad \text{Eq.7}$$

Where Y_{fuel} denotes the fuel mass fraction, and R_{fuel} represents the fuel reaction rate.

Mixture mass fraction transport equation.

$$\frac{\partial}{\partial t}(\beta_v \rho \xi)+\frac{\partial}{\partial x_j}(\beta_j \rho u_j \xi)=\frac{\partial}{\partial x_j}\left(\beta_j \frac{\mu_{\text{eff}}}{\sigma_\xi}\frac{\partial \xi}{\partial x_j}\right) \quad \text{Eq.8}$$

Where the value of σ_ξ is set to 0.7.

2.2.2 Turbulence model

The standard k-ε two-equation turbulence model is employed for the numerical simulations. This model introduces two supplementary transport equations to compute the turbulent kinetic energy (k) and the turbulent dissipation rate (ε), in accordance with the eddy viscosity hypothesis.

Turbulent kinetic energy transport equation.

$$\frac{\partial}{\partial t}\left(\beta_v \rho k\right)+\frac{\partial}{\partial x_j}\left(\beta_j \rho u_j k\right)=\frac{\partial}{\partial x_j}\left(\beta_j \frac{\mu_{\mathrm{eff}}}{\sigma_k}\frac{\partial k}{\partial x_j}\right)+\beta_v P_k-\beta_v \rho \varepsilon \qquad \text{Eq.9}$$

Where the value of σ_k is set to 1.

Turbulent dissipation rate transport equation.

$$\frac{\partial}{\partial t}\left(\beta_v \rho \varepsilon\right)+\frac{\partial}{\partial x_j}\left(\beta_j \rho u_j \varepsilon\right)=\frac{\partial}{\partial x_j}\left(\beta_j \frac{\mu_{\mathrm{eff}}}{\sigma_\varepsilon}\frac{\partial \varepsilon}{\partial x_j}\right)+\beta_v P_\varepsilon-C_{2\varepsilon}\beta_v \rho \frac{\varepsilon^2}{k} \qquad \text{Eq.10}$$

In the formula, set $C_{2\varepsilon}$ to 1.92 and set σ_ε to 1.3.

3 Model validation

Hou (2023) constructed a scaled experimental model, as illustrated in Fig. 2, to validate the reliability of numerical simulation results while investigating the hydrogen leakage and diffusion behavior within the passenger cabin of a hydrogen fuel cell bus. The experimental model consists of a rectangular enclosure measuring 1.7 m × 0.48 m × 0.4 m. Helium was employed as a surrogate gas in the leakage and diffusion tests due to its comparable physical properties, given the safety hazards associated with hydrogen. The leakage parameters for both the experimental and simulation scenarios were determined based on the hydrogen-helium diffusion similarity theory. In the numerical simulation, the hydrogen leakage mass flow rate was set to 9.24×10^{-6} kg/s. The experiment was divided into two stages, including a 120 s continuous leakage phase, followed by a 120 s free diffusion phase after the leakage source was shut off. Three monitoring points were installed within the model at coordinates S1(0, −0.35, 0.4), S2(0, 0.35, 0.4), and S3(−0.24, 0, 0.36). The specific location and dimensions of the leak orifice are detailed in Fig. 2. In this study, an identical computational model was developed using CFD (Fig. 3), with the monitoring point layout strictly consistent with the referenced literature. The simulation results from the initial 120 s of the leakage phase were selected to validate the numerical model, balancing computational efficiency with practical operating constraints.

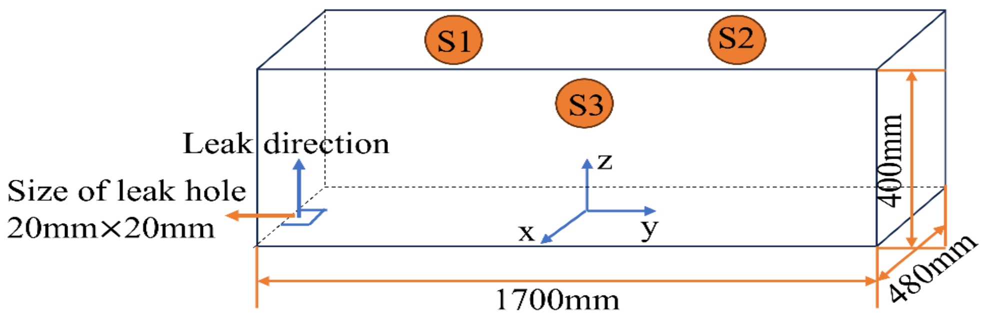

Fig. 2 Physical model for helium leakage and dispersion experiments

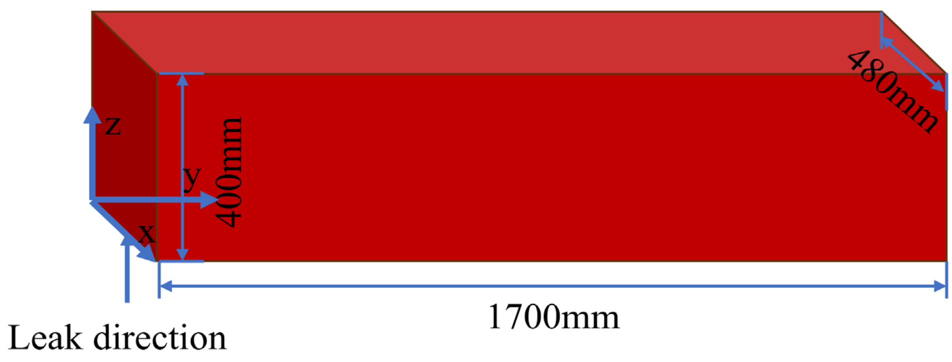

Fig. 3 Physical model for hydrogen leakage and dispersion simulation

Fig. 4 shows the experimental and simulation results of the hydrogen volume fraction at each monitoring point. The comparison reveals that the trends of the experimental and simulation results are in good agreement, indicating that the CFD software exhibits high accuracy and reliability in simulating the hydrogen leakage and dispersion process.

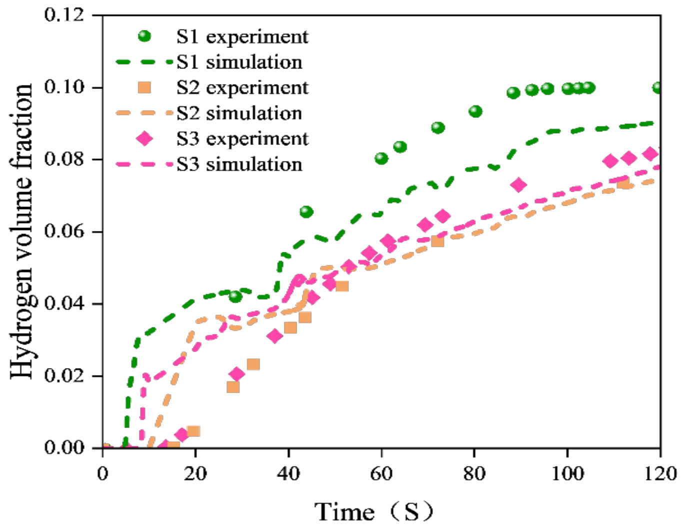

Fig. 4 Figure showing the validation results of the leakage diffusion model

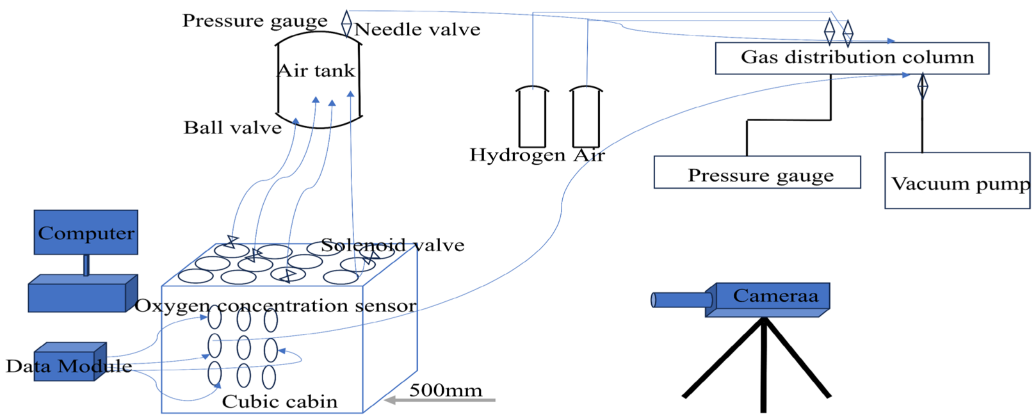

Fig. 5 Hydrogen Explosion Experiment Device

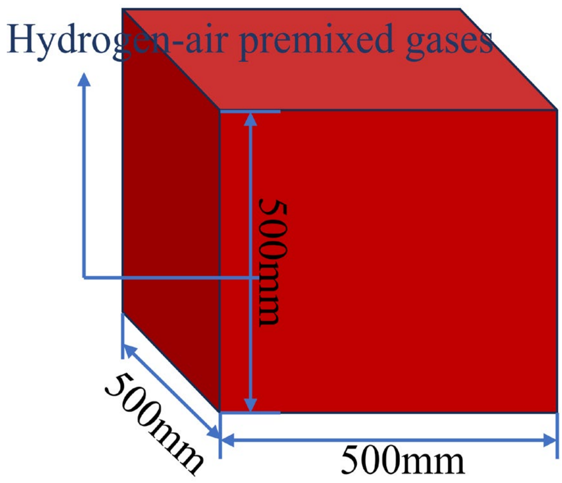

Fig. 6 Physical model for hydrogen explosion

Han (2019) investigated the explosion characteristics of hydrogen at varying concentrations within a cubic chamber with a side length of 0.5 m. The initial concentrations were established by introducing different volumes of hydrogen into the chamber, with ignition initiated at its center. The experimental setup is illustrated in Fig. 5. The experimental procedure primarily consists of three stages: preparation and filling, gas mixing, and ignition with data acquisition. First, the gas distribution system is utilized to evacuate the gas storage tank before filling it with pure hydrogen. Simultaneously, the explosion chamber is evacuated and then filled with dry air at atmospheric pressure, with one of the bottom side openings kept open as an exhaust vent. Subsequently, six ball valves surrounding the storage tank are opened, and an electronic relay is employed to precisely control the gas injection duration. Once the injection is complete, the opened ball valves are closed. For homogeneous mixture ignition tests, the circulation system valves and the circulation pump are activated to mix the gas within the chamber prior to ignition. Conversely, for ignition tests involving concentration gradients, the plug is tightly closed to allow hydrogen to diffuse naturally, and the experiment proceeds once the desired concentration gradients are established. Finally, when the gas mixture in the explosion chamber meets the experimental requirements, ignition is initiated using a high-voltage ignition system. Concurrently, the camera system is triggered to record the event, and pressure data are acquired. All recorded data are promptly saved upon completion.

A 1:1 scale model was constructed in CFD, with the monitoring point layout identical to that of the experimental setup. The maximum hydrogen leakage duration in this study was set to 60 s. The hydrogen volume fraction within the cabin reached 18.1% following complete mixing under confined conditions. To validate the reliability of the numerical model, the explosion overpressure data following ignition under homogeneous conditions at hydrogen volume fractions of 12.1% and 22.2%, as reported by Han (2019), were selected for comparative validation. The ignition location was kept consistent with the experiments, positioned at the center of the cubic chamber. The comparison between the numerical simulation results and the experimental data is presented in the figure.

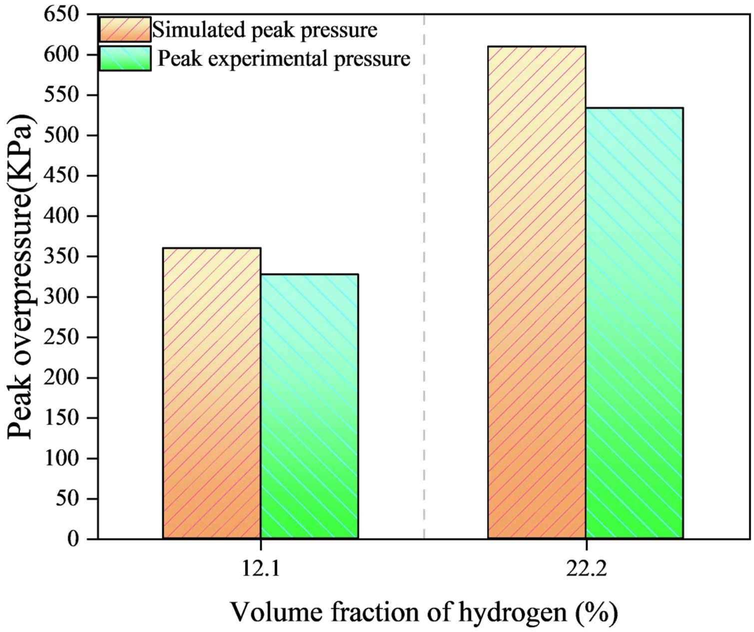

Fig. 7 Comparison of simulated and experimental peak overpressure results

As shown in Fig. 7, simulated peak overpressures slightly exceed experimental measurements across all tested hydrogen volume fractions, primarily due to minor sealing imperfections, wall heat dissipation, and imperfect gas mixing. Nevertheless, CFD simulation software closely reproduces the experimental trends with strong quantitative agreement, validating the model's reliability in predicting hydrogen–air combustion and explosion dynamics.

4 Mesh independence analysis

Mesh quality significantly influences numerical simulation results. Both mesh size and the number of elements not only directly dictate computational accuracy but also substantially impact computational cost. An appropriate mesh resolution must be carefully selected to balance these factors, ensuring reliable simulation outcomes within a reasonable computational timeframe. Conducting a mesh independence analysis is an essential step to ensure both the accuracy of the simulation results and computational efficiency.

Mesh refinement near the leak source is required for simulating flammable gas leaks. The grid size must satisfy the single-cell resolution criterion within the expansion jet region at ambient pressure. Whereas for high-buoyancy, low-momentum release gases a stricter meshing criterion must be followed. A local mesh refinement was implemented in the vicinity of the leak orifice in this study. To assess grid independence, three computational meshes were generated with baseline cell sizes of 125 mm, 100 mm and 75 mm, respectively, outside the locally refined regions. Three monitoring points were placed in each mesh configuration to investigate the temporal evolution of the hydrogen volume fraction across different grid resolutions. The simulation results at each monitoring point are presented in the figure.

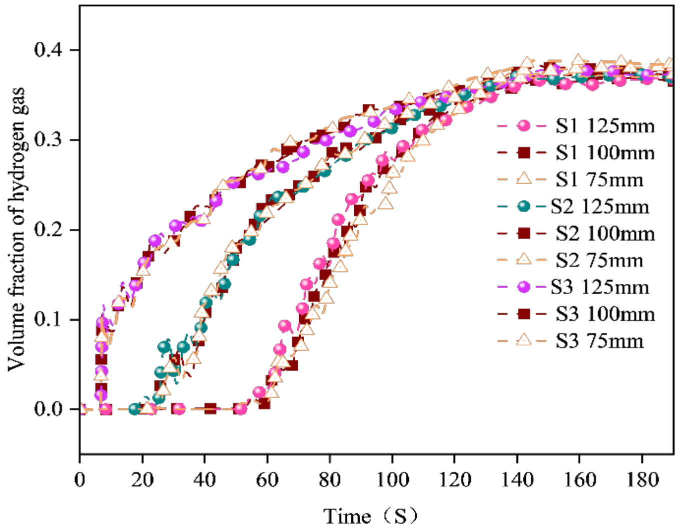

Fig. 8 Variation curves of hydrogen volume fraction at different grid resolutions

As shown in Fig. 8, with the local refinement zone near the leak orifice fixed at 112 mm, the temporal evolution of the hydrogen volume fraction at the three monitoring locations remains virtually identical across background mesh sizes of 125, 100 and 75 mm. Balancing computational accuracy and cost, the mesh size for the core refined region is ultimately selected as 112 mm, while that for the remaining regions are set to 125 mm.

In explosion simulations, the combustion zone should be discretized using hexahedral mesh cells. Typically, a grid aspect ratio deviation within 10% is considered acceptable. In this study, a mesh independence analysis was conducted for the explosion scenario. Ignition was initiated in the formed gas cloud 30 s after the leak began, with the ignition source positioned at the geometric center of the bus passenger compartment. All windows were simplified as pressure relief surfaces. Fig. 9 presents the pressure-time histories at the same monitoring point for total mesh counts of 354,816, 403,340, and 509,496.

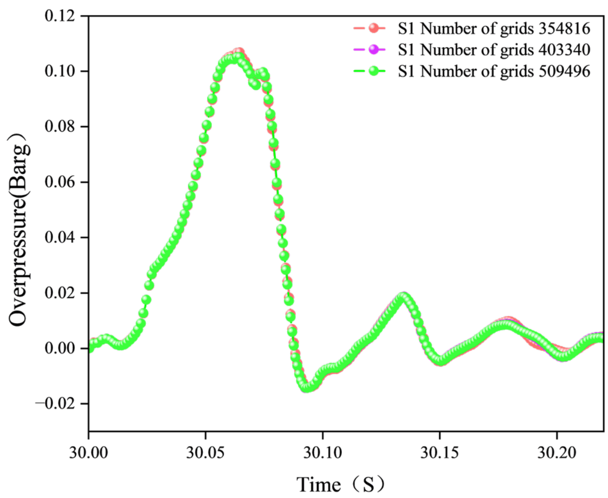

Fig. 9 Maximum overpressure curves for hydrogen explosions at different grid resolutions

The calculated pressure at the monitoring point converges once the total number of computational cells reaches 403,340. Further mesh refinement yields only marginal improvements in computational accuracy. Considering the trade-off between computational cost and solution efficiency, this study ultimately adopts a total of 403,340 mesh elements for the explosion process.

5 Diffusion and explosion simulation

The present numerical simulation study primarily comprises two parts. The first section investigates hydrogen leakage and dispersion within a hydrogen-powered bus, specifically examining the influence of window opening configurations, the number of open windows, dispersion duration, and ambient wind direction on the spatial distribution of hydrogen concentration within the passenger compartment. In the leakage scenario, the center of the leakage source is located at coordinates (1.25, 5.25, 0), and the leakage direction is oriented along the positive z-axis. The second part aims to simulate the ignition and explosion of the leaked gas cloud, exploring the characteristics of the overpressure and high-temperature fields generated under varying initial hydrogen concentrations, and evaluating the potential injury risks to occupants. To comprehensively capture the spatiotemporal evolution of the physical fields during the leakage, dispersion, and explosion phases, 102 monitoring points were distributed within and in the vicinity of the bus cabin, as illustrated in Fig. 10.

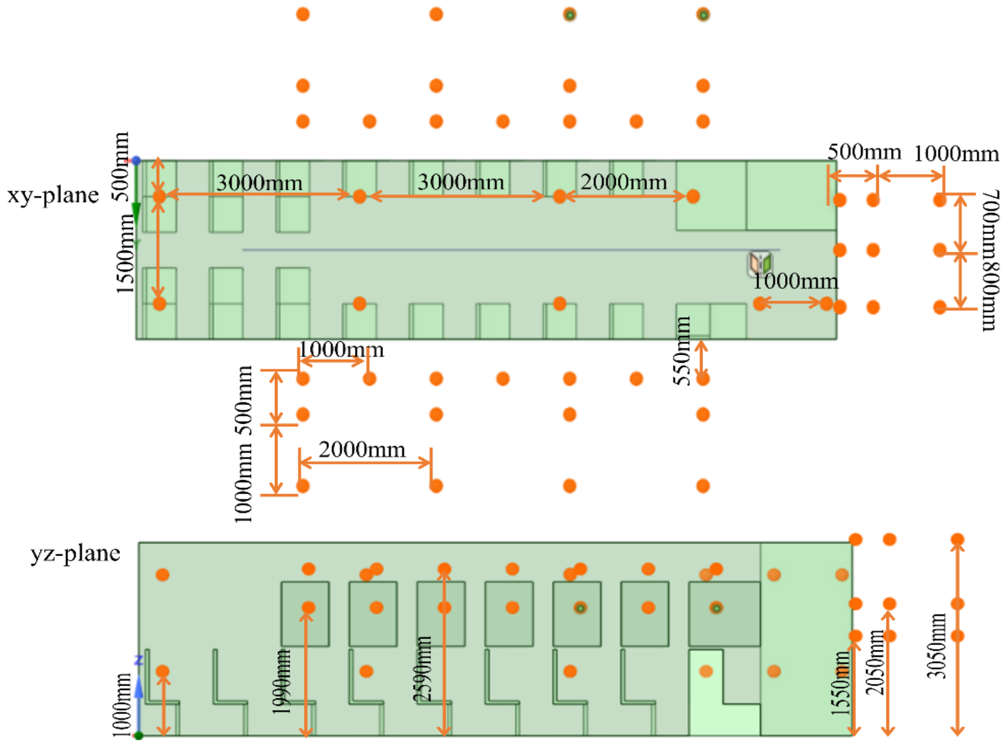

Fig. 10 Distribution of monitoring points

5.1 Effect of ventilation and window opening configurations on hydrogen leak dispersion

The case designations are detailed in Table 1. The bus window regions are modeled as solid wall boundaries in the numerical simulation of hydrogen leakage and dispersion under confined conditions. The leakage initiation time is set at 0 s with a duration of 60 s, and flow field data are output at 10 s intervals during the simulation to support subsequent explosion analyses. A total simulation duration of 60 s is implemented for the remaining cases, consisting of a 30 s leakage phase followed by source termination and a subsequent 30 s dispersion period. The concentration field data of the hydrogen cloud at t = 30 s are extracted for subsequent ignition and explosion simulations.

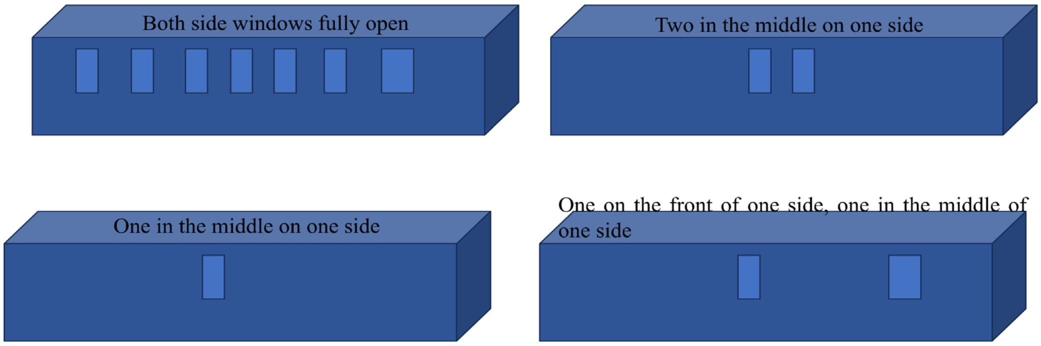

Fig. 11 Physical models of different window opening configurations

Table 1 Description of Various Operating Conditions

Serial number	Window Opening Method	Wind direction	Wind speed（m/s）
Case1	Fully open	nothing	0
Case2	Fully open	x	2
Case3	Fully open	y	2
Case4	Two in the middle on one side	nothing	0
Case5	Two in the middle on one side	x	2
Case6	One in the middle on each side	nothing	0
Case7	One in the middle on each side	x	2
Case8	One on the front of one side, one in the middle of one side.	nothing	0
Case9	One on the front of one side, one in the middle of one side.	x	2
Case10	Fully closed	nothing	0

The two-dimensional planar and three-dimensional spatial distribution maps of the flammable gas at different time points following leakage under confined conditions are shown below.

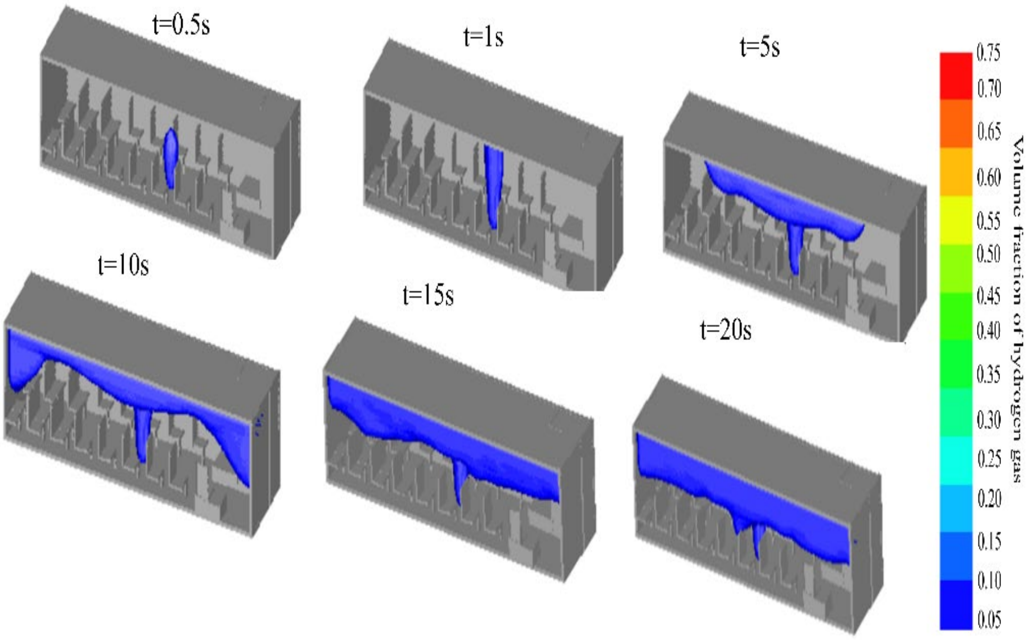

Fig. 12 Distribution of flammable hydrogen gas clouds within the cabin at different time instants

As shown in Fig. 12, hydrogen reaches the ceiling at approximately 1 s following ejection from the leak orifice, subsequently spreading horizontally across the ceiling surface. At approximately 5 s, hydrogen completely covers the ceiling region along the x-direction. Thereafter, the hydrogen spreads downward along the side walls and the front and rear end walls of the bus, gradually diffusing from the wall surfaces toward the central region of the passenger compartment.

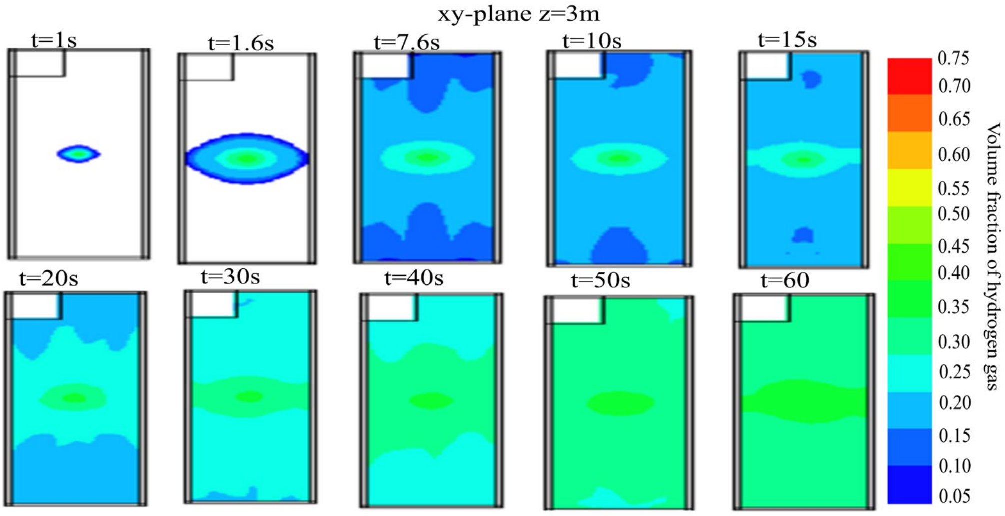

Fig. 13 Distribution of flammable hydrogen on the xy-plane at different time instants

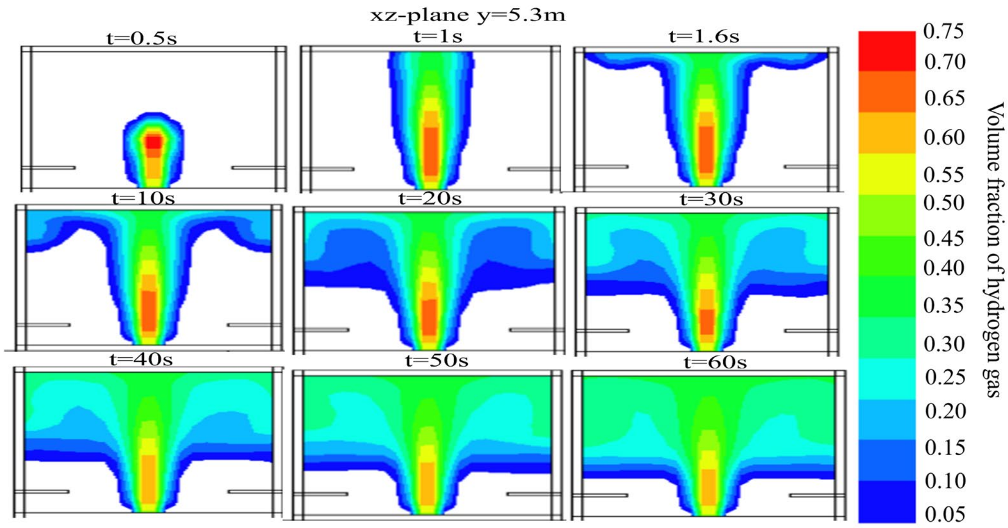

Fig. 14 Distribution of flammable hydrogen on the xz-plane at different times

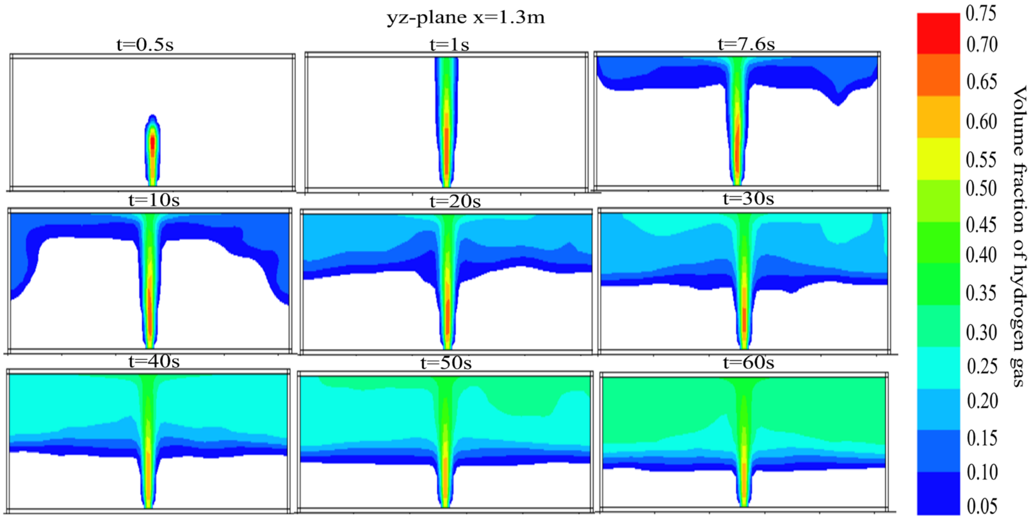

Fig. 15 Distribution of flammable hydrogen on the yz-plane at different times

The hydrogen jet reaches the ceiling approximately 1 s after release from the leak orifice, and subsequently spreads laterally along the horizontal plane (xy-plane). By 1.6 s, the hydrogen layer near the ceiling has reached the left and right side walls of the bus. By 7.6 s, it further extends to the front and rear end walls. As the leakage progresses, hydrogen gradually descends and diffuses into the lower compartment. The concentration distributions on the xy-plane indicate that the hydrogen concentration at a given height tends toward uniformity over time, whereas in the vertical direction, a pronounced concentration stratification is observed across different height levels.

The locations of various monitoring points within the passenger compartment, along with the temporal variation of the hydrogen volume fraction over the leakage duration, are presented in Table 2 and Fig. 16.

Table 2 Monitoring point

Monitoring point	X	Y	Z
S2	0.5	0.35	2.5
S6	0.5	6.35	2.5
S10	2	0.35	2.5
S3	0.5	3.35	1
S7	0.5	8.35	1
S11	2	3.35	1

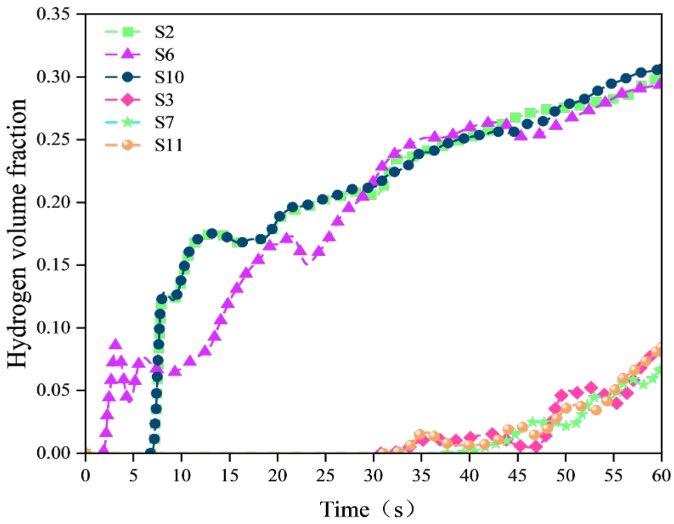

Fig. 16 Variation curves of hydrogen volume fraction at different measurement points

As shown in the figure, during a hydrogen leak in the cabin, the hydrogen concentrations at monitoring points located at the same height gradually become uniform as the leakage duration increases, whereas significant differences are observed at different heights. This result indicates that the hydrogen concentration exhibits pronounced vertical stratification.

Table 3 Monitoring point

Monitoring point	X	Y	Z
S10	2	0.35	2.5
S12	2	3.35	2.5
S14	2	6.35	2.5
S16	2	9.35	2.5
S18	2	10.35	2.5

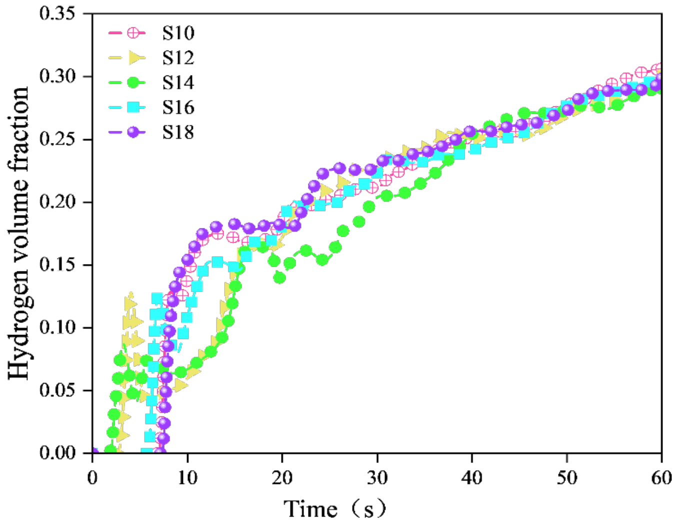

Fig. 17 Variation curves of hydrogen volume fraction at different measurement points

Fig. 17 illustrates the temporal evolution of the hydrogen volume fraction at monitoring points located at various y-coordinates along the line defined by x=2 and z=2.5. As shown, the hydrogen volume fraction in the region adjacent to the leak orifice increases first, reaching the lower explosive limit (LEL) of hydrogen during the initial stage of leakage. By 8 s into the leakage event, the hydrogen volume fractions at all monitoring points on this plane have reached the LEL. Furthermore, the variation trends near both side walls are largely consistent. Ultimately, the hydrogen volume fractions at all monitoring points on the same horizontal plane tend to become uniform.

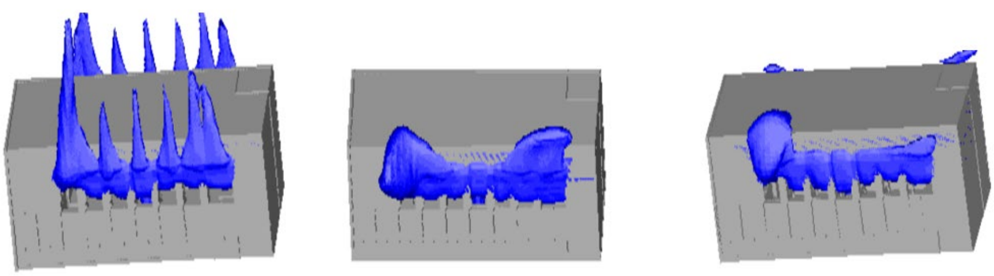

Fig. 18 Distribution of hydrogen gas clouds outside the cabin under different

ventilation modes

Taking the fully opened windows scenario as an example, Fig. 18 employs a three-dimensional volumetric plot to illustrate the influence of wind direction on the distribution of the gas cloud outside the passenger compartment. As shown, the ambient wind field—encompassing both the presence or absence of wind and variations in wind direction—exerts a significant impact on the spatial distribution of the flammable gas cloud outside the compartment. Hydrogen escaping through the windows disperses predominantly upward above the bus under no-wind conditions, driven by buoyancy effects. Hydrogen is advected downwind under an applied x-direction wind field, thereby preventing the formation of a flammable cloud on the leeward side of the vehicle. Similarly, under a y-direction wind field, the hydrogen migrates toward the downwind side, with no flammable hydrogen cloud observed in the frontal region of the bus.

The distribution characteristics of the flammable hydrogen cloud within the passenger cabin and the hydrogen concentrations at each monitoring point are presented below for all operating conditions, excluding the confined scenario.

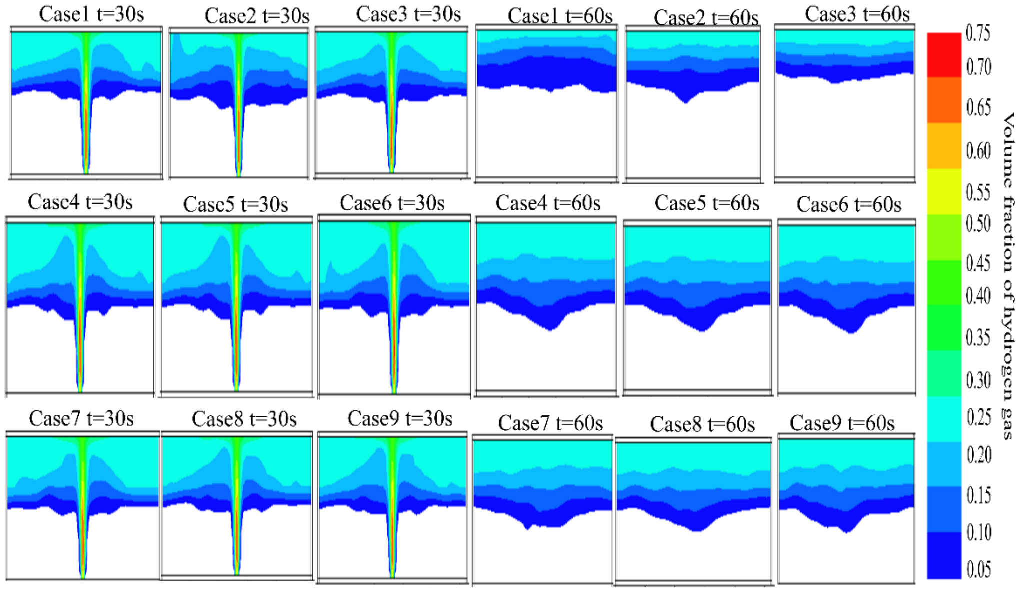

Fig. 19 Contour plots of hydrogen distribution on different yz-planes under various operating conditions at different time instants

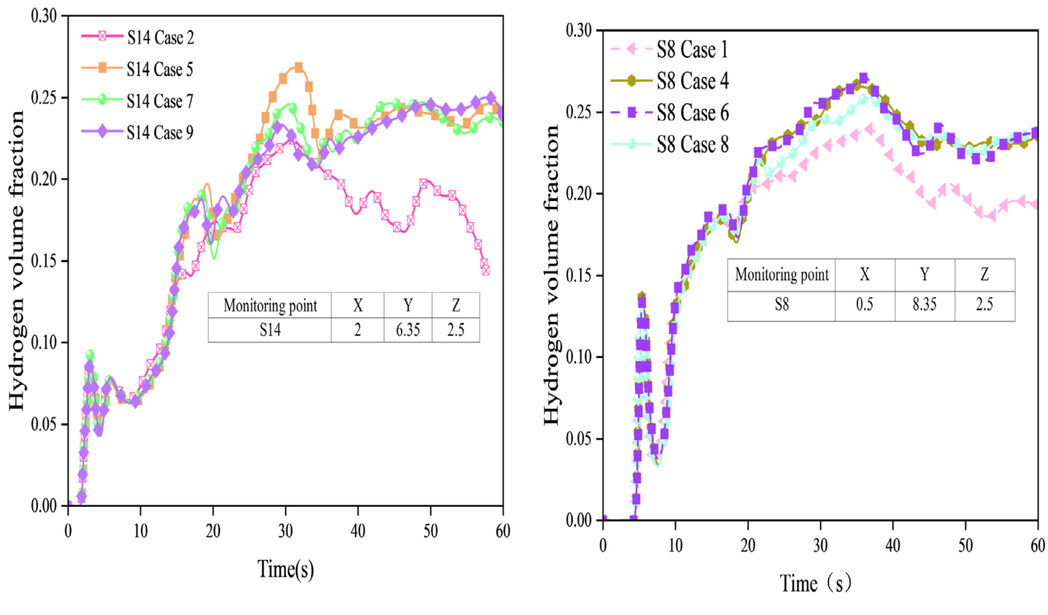

Fig. 20 Variation curves of hydrogen concentration at the same measurement point under different operating conditions

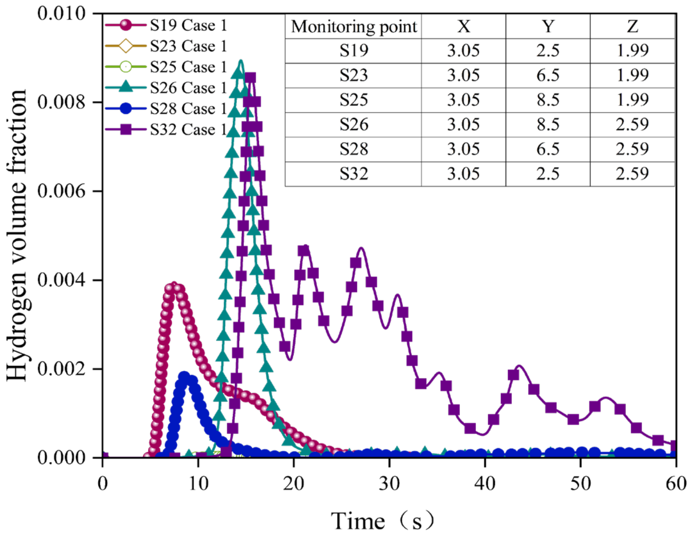

Fig. 21 Hydrogen concentration variation curves at different measurement points under the same operating condition

As illustrated in the figure above, the number of open windows exerts a significant influence on the hydrogen volume fraction at monitoring point S8. Conversely, variations in window opening positions exert a negligible influence on the hydrogen volume fraction at S8, provided that the number of open windows remains constant. The external hydrogen cloud predominantly accumulates in the region above the windows, whereas the concentration of combustible gas in the middle and lower sections of the windows remains relatively low. The hydrogen cloud distribution within the passenger cabin remains largely unaffected under either zero-wind conditions or a y-directional wind field. This is primarily attributed to the blocking effect of the front windshield against y-directional airflow. In contrast, airflow along the x-direction can directly penetrate the cabin through the open windows, thereby substantially altering the spatial distribution characteristics of the internal hydrogen cloud. The hydrogen volume fraction within the cabin at 60 s decreases as the number of open windows increases under x-directional ambient wind conditions. The hydrogen volume fraction is higher in single-side opening configurations than in bilaterally symmetric arrangements, with positional variations exerting only a marginal influence, for scenarios involving exactly two open windows. In the event of a hydrogen leak, all cabin windows should be opened immediately to reduce the internal hydrogen volume fraction. Furthermore, the presence of ambient wind can expedite the diffusion and dissipation of the external combustible gas cloud.

5.2 Analysis of combustion and explosion results under different ignition conditions

The numerical simulation of the explosion presented herein is based on the following assumptions, (1) radiative heat transfer losses are neglected, (2) the primary structure of the hydrogen-fueled bus possesses sufficient strength to withstand the maximum overpressure generated by the explosion, while windows are modeled as explosion venting panels and the pressure relief panel is configured with an activation pressure of 3.5 kPa. The glass shatters instantaneously and completely once the venting activation threshold is reached. The spatial arrangement of the venting panels is illustrated in Fig. 22. During the explosion simulation phase, the hydrogen cloud resulting from the leakage is ignited. The ignition source is positioned at the geometric center of the passenger compartment to evaluate the hazardous effects of hydrogen ignition and subsequent explosion under varying leakage durations. Table 4 and Table 5 present the corresponding damage levels to human occupants and building structures at various overpressure and temperature thresholds, respectively.

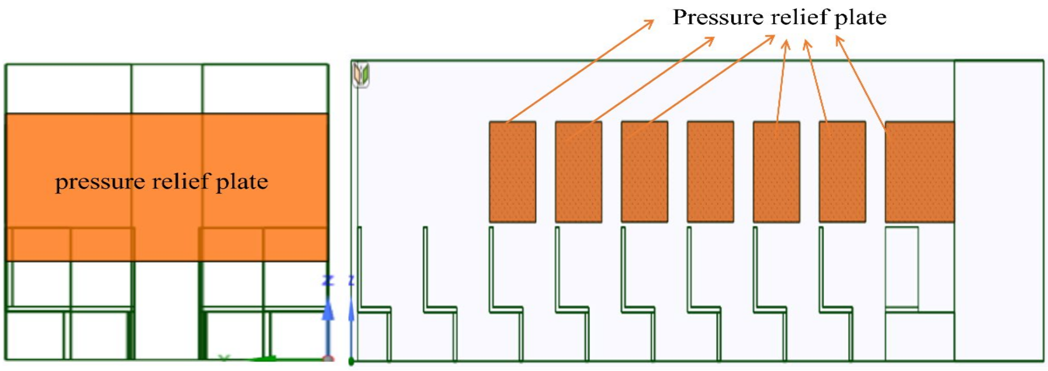

Fig. 22 Distribution of pressure relief panels on hydrogen fuel cell buses

Table 4 Assessment criteria for overpressure-induced injury（Fu et al.,2009；Shu,2023).

Overpressure（Bar）	Degree of harm to the human body	Extent of damage to buildings
<0.2	Basic safety of personnel	Doors and windows are damaged.
0.2-0.3	Minor injury (slight damage to the human body)	Cracks in building walls
0.3-0.5	Moderate injury (damaging of the auditory organs or fractures)	The cracks in the building walls have deepened and widened, with roof tiles falling off.
0.5-1	Severe injury (significant damage to internal organs or even death)	The building structure is loose, and the brick walls have collapsed.
>1	Death-related injuries (most cases resulted in fatalities)	The reinforced concrete suffered severe damage, small buildings collapsed, and large steel frame structures were destroyed.

Table 5 Diagnostic criteria for heat-related injurie(Shu,2023).

Temperature （K）	The detrimental effects of high temperatures on human health and buildings
315	Feeling pain
391	Critical injury temperature of the human body
453	Temperatures causing severe harm to the human body
673	A portion of the steel structure has failed.
873	The entire steel structure has failed completely.

The temperature distribution analysis is conducted on the cross-section at z = 1.3 m. This height is selected because it provides a clear visualization of the temperature distribution across all passenger seats in the cabin. Moreover, it approximately corresponds to the upper torso level of a seated adult passenger, where vital organs are located, thereby enabling an effective evaluation of the thermal hazards to human occupants. As shown in Fig. 23, during the initial ignition phase, the temperature variations of the gas cloud at the z = 1.3 m cross-section exhibit minimal differences across different leakage initiation times. As time progresses, longer leakage durations result in more pronounced temperature changes and a correspondingly faster rate of temperature rise. Furthermore, the temperature propagation speed in the negative y-direction from the ignition source is lower than that in the positive y-direction during the early ignition stage. This asymmetry is attributed to the higher obstacle density in the rear cabin compared to the front. The peak post-ignition temperatures exceed 2000 K across all leakage scenarios, far surpassing the human thermal tolerance threshold and representing an unacceptably severe hazard.

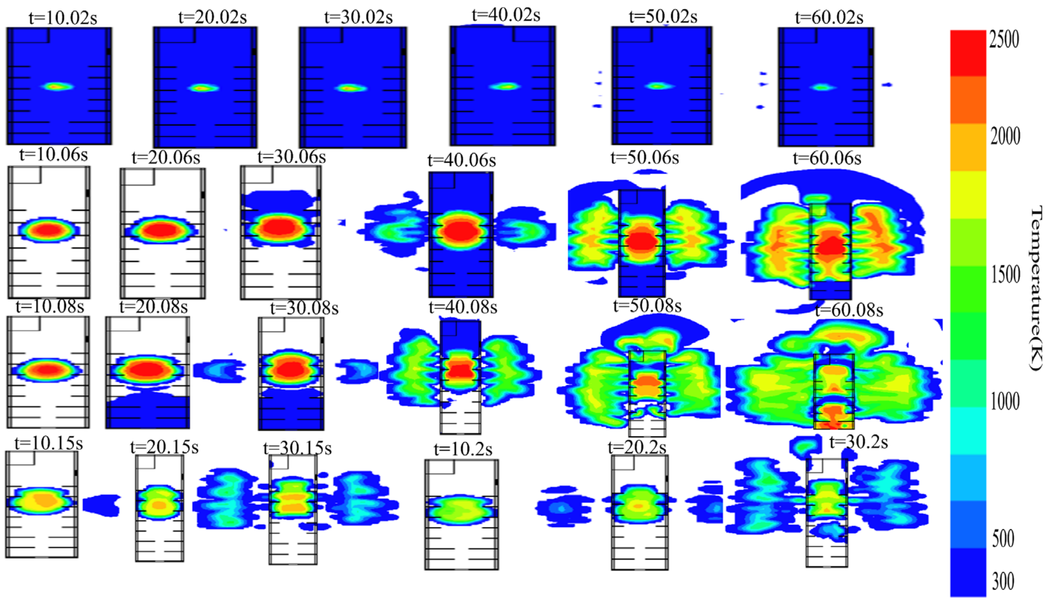

Fig. 23 Temperature distribution in the xy-plane at different ignition timings

The gas cloud generated by a 60s leak was ignited under confined conditions. Figure 24 illustrates the temporal evolution of the flame volume at temperatures exceeding 873 K.

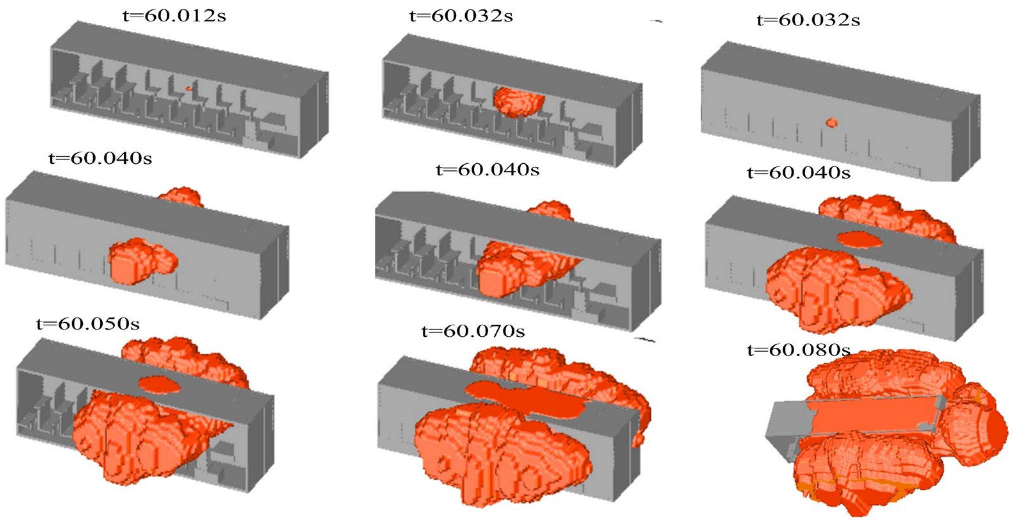

Fig. 24 Flame graphs at different time points

As shown in the Fig. 24 ,the temperature near the ignition source rises to 873 K after ignition 12 ms. The flame propagates to the mid-section windows of the bus by 32 ms. As the window glass functions as a pressure-relief component, the flames rapidly vent outward through the window openings. The central passenger compartment is completely engulfed by flames at 50 ms, which also extend to the front windshield. The fire further expands into the external environment through the side windows and the front windshield by 70 ms. The steel structure has completely lost its load-bearing capacity at 873 K, and this temperature far exceeds the human physiological tolerance limit. The passenger compartment is exposed to extreme heat within tens of milliseconds following hydrogen ignition, affording occupants virtually no time for effective response or evacuation.

Fig. 25 presents the temperature contour plots at selected time intervals following ignition under Case 2 conditions.

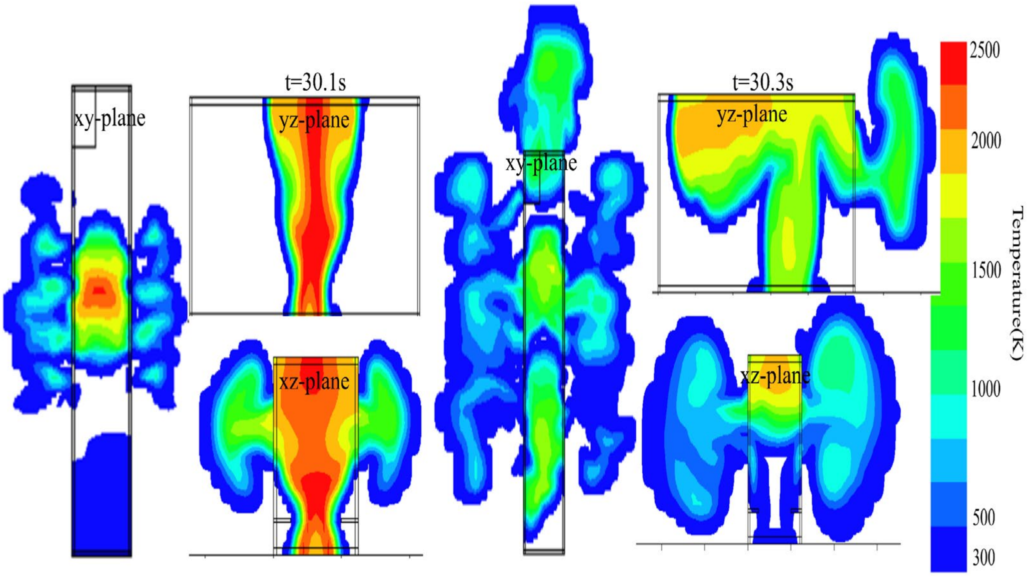

Fig. 25 Temperature contour plots at different time instants after ignition

Ignition triggers the rapid propagation of high-temperature flames throughout the passenger compartment following 30 s of continuous hydrogen leakage. The explosion-induced overpressure shatters the side windows and front windshield, followed by the outward propagation of high-temperature flames from the vehicle. The entire process lasts less than 1 s, resulting in severe damage to both the cabin interior and the surrounding environment.

The results obtained from the explosion monitoring points under different operating conditions, along with the corresponding maximum overpressures, are shown in the figure below.

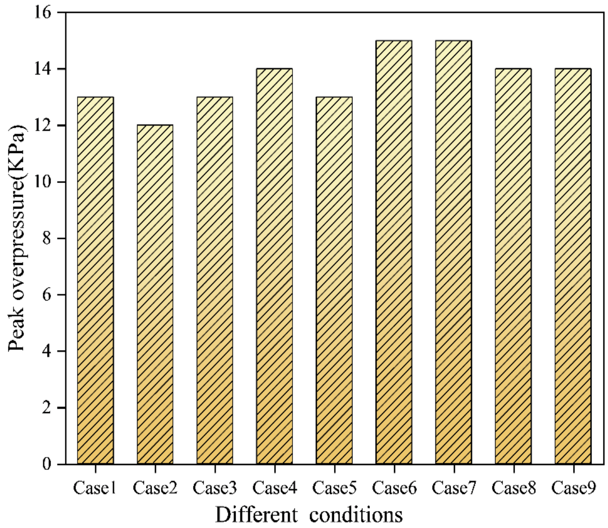

Fig. 26 Maximum overpressure generated by hydrogen explosions under different operating conditions

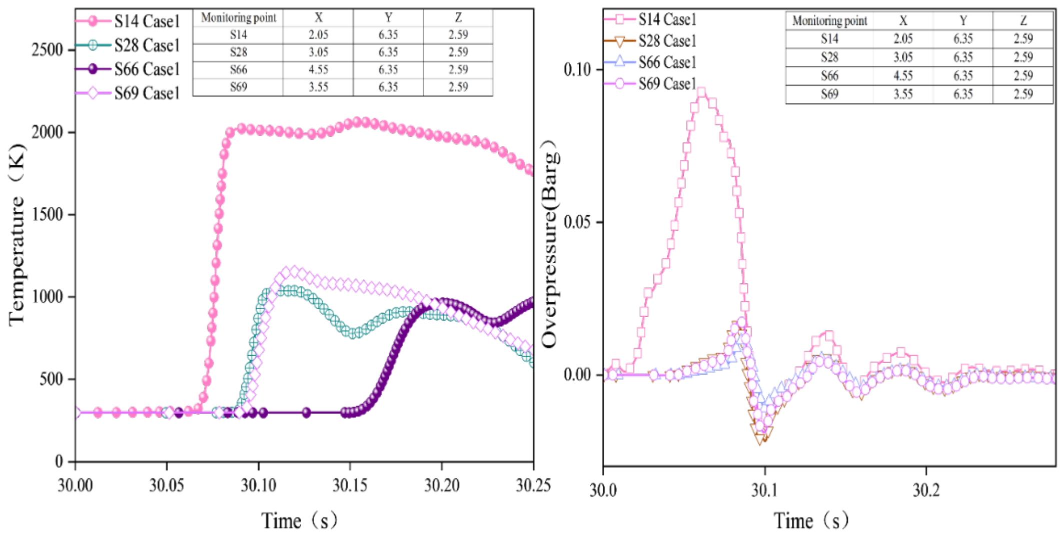

Fig. 27 Temperature and pressure variation curves at different measurement points

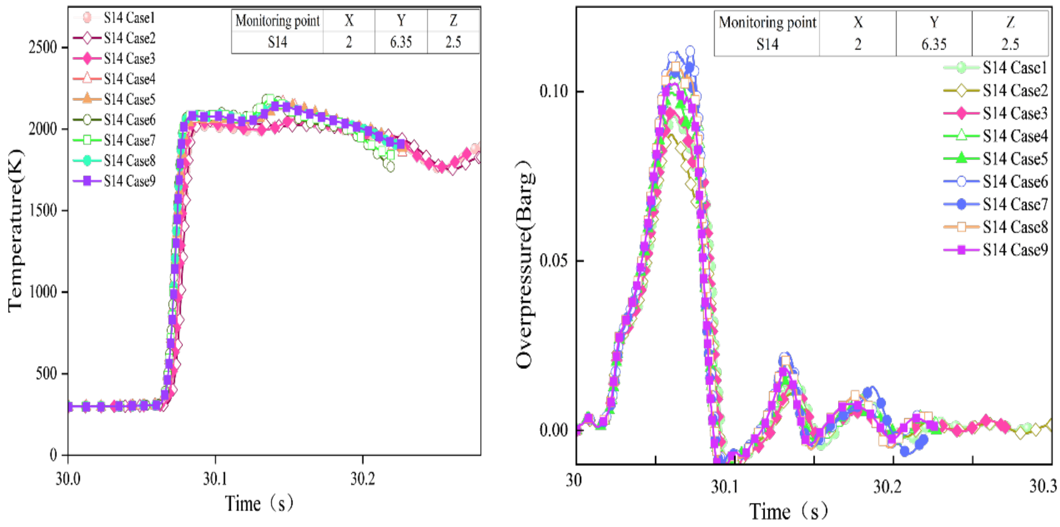

Fig. 28 Temperature and pressure variation curves under different operating conditions at the same measurement point

The window opening configurations and quantities primarily influence the peak temperature and overpressure during the combustion and explosion process by modulating the hydrogen diffusion concentration within the passenger cabin. Window arrangements and ventilation patterns that facilitate hydrogen venting can significantly reduce the maximum overpressure and peak temperature inside the bus cabin as illustrated in the figure. Both overpressure and temperature decrease significantly with increasing distance from the cabin under identical operating conditions. The maximum overpressures at all interior and exterior monitoring points remain relatively low during a 30 s hydrogen leakage event, attributable to the explosion-venting effect of the bus's multi-window structure, which minimizes the risk of blast-induced injury to occupants. However, the peak temperature within the cabin can exceed 2000 K, and even at a distance of 2 m from the exterior wall, the maximum temperature can still reach 1000 K. Based on the time-history curves of pressure and temperature at the monitoring points shown in Fig. 27 and Fig.28, it can be observed that under the investigated conditions, the maximum overpressure remains consistently below the lower limit of human tolerance (0.2 bar（Fu et al.,2009；Shu,2023)). In contrast, the temperature at the monitoring points surges to approximately 2000 K instantaneously during the deflagration, far exceeding the critical threshold (453 K(Shu,2023)) for severe human tissue injury. Although hydrogen deflagration is a transient event lasting only 200–300 ms, the temperature at 300 ms remains significantly higher than the safe human exposure limit. Furthermore, the residual heat continues to pose a thermal hazard for a certain period after the deflagration ceases. Therefore, by comprehensively considering the peak temperature, peak overpressure, and their respective exposure durations, it can be concluded that under the investigated conditions, the thermal hazard to the human body is significantly greater than the overpressure hazard.

6 Conclusion

This study employs the CFD to numerically simulate the leakage and dispersion of hydrogen within the passenger cabin of a hydrogen fuel cell bus under various operating conditions. Ignition scenarios are also defined to investigate the potential hazards following the accidental ignition of the gas cloud. The main conclusions are as follows.

1. The severity of thermal hazards exceeds that of overpressure hazards in fire and explosion incidents resulting from accidental hydrogen leakage from fuel cell buses, under the operating conditions specified in this study.

2. Simulation results indicate that during hydrogen leakage, the hydrogen concentration within the passenger compartment of a hydrogen fuel cell bus exhibits a pronounced stratified

distribution along the vertical direction. Within the same horizontal plane, hydrogen concentrations at various monitoring points gradually tend toward uniformity as the leakage duration increases, whereas significant concentration differences persist among monitoring points at different heights.

3. Analysis of the post-ignition evolution of hydrogen temperature contours indicates that the dense obstacle distribution in the rear cabin significantly reduces the temperature rise rate in that region compared to the front section. Consequently, when the front cabin temperature exceeds 1000 K, the rear section remains within the safety threshold.

4. The peak temperature exceeds 1000 K at a distance of 2 m in the x-direction from the bus window following the explosion of a hydrogen cloud generated by a 30-s leak, posing a severe thermal hazard to nearby personnel.

Acknowledgements

The work is supported by the Program for Science & Technology Innovative Research Team in the University of Henan Province (25IRTSTHN005) and the Fundamental Research Funds for the Universities of Henan Province.

Declaration of competing interest

The authors have no competing interests to declare that are relevant to the content of this article.

References

Chen, M., Zhao, C., Sun, F., et al. 2020. Research progress of catalyst layer and interlayer interface structures in membrane electrode assembly (MEA) for proton exchange membrane fuel cell (PEMFCs) system. ETransportation. 5: 100075.

Cui, S., Zhu, G., He, L., et al. 2023. Analysis of the fire hazard and leakage explosion simulation of hydrogen fuel cell vehicles. Thermal Science and Engineering Progress. 41: 101754.

Fu, Z.M., Huang, J.Y., Zang, N. 2009. Quantitative analysis on the damage effect of explosion shock wave. Fire Science and Technology. 28(06): 390-395.

Guo, L., Su, J., Wang, Z., et al. 2024. Hydrogen safety: An obstacle that must be overcome on the road towards future hydrogen economy. International Journal of Hydrogen Energy. 51: 1055-1078.

Han, S. 2019. Study on explosion characteristics of hydrogen with concentration gradient in cubic cabin. Hefei University of Technology.

Hou, X.L. 2023. Study on hydrogen leakage diffusion and ventilation scheme in the passenger compartment of hydrogen fuel cell buses. Beijing University of Technology.

Khalil, Y.F. 2018. Science-based framework for ensuring safe use of hydrogen as an energy carrier and an emission-free transportation fuel. Process Safety and Environmental Protection. 117: 326-340.

Kulikovsky, A. 2019. A model for concentration impedance of a PEM fuel cell. ETransportation. 2: 100026.

Li, Z., Wu, J., Liu, M., et al. 2019. Numerical analysis of the characteristics of gas explosion process in natural gas compartment of utility tunnel using FLACS. Sustainability. 12(1): 153.

Lucas, M., Atanga, G., Hisken, H., et al. 2021. Simulating vented hydrogen deflagrations: Improved modelling in the CFD tool FLACS-hydrogen. International Journal of Hydrogen Energy. 46(23): 12464-12473.

Lu, Y., Fan, R., Wang, Z., et al. 2024. The influence of hydrogen concentration on the characteristic of explosion venting: explosion pressure, venting flame and flow field microstructure. Energy. 293: 130562.

Lynch, S.P. 2011. Hydrogen embrittlement (HE) phenomena and mechanisms. In: Stress corrosion cracking. Woodhead Publishing, pp. 90-130.

Malakhov, A.A., Avdeenkov, A.V., Du Toit, M.H., et al. 2020. CFD simulation and experimental study of a hydrogen leak in a semi-closed space with the purpose of risk mitigation. International Journal of Hydrogen Energy. 45(15): 9231-9240.

Mao, X., Ying, R., Yuan, Y., et al. 2021. Simulation and analysis of hydrogen leakage and explosion behaviors in various compartments on a hydrogen fuel cell ship. International Journal of Hydrogen Energy. 46(9): 6857-6872.

Mogi, T., Kim, D., Shiina, H., et al. 2008. Self-ignition and explosion during discharge of high-pressure hydrogen. Journal of Loss Prevention in the Process Industries. 21(2): 199-204.

Moradi, R., Groth, K.M. 2019. Hydrogen storage and delivery: Review of the state of the art technologies and risk and reliability analysis. International Journal of Hydrogen Energy. 44(23): 12254-12269.

Najjar, Y.S.H. 2013. Hydrogen safety: The road toward green technology. International Journal of Hydrogen Energy. 38(25): 10716-10728.

Roes, A.L., Patel, M.K. 2011. Ex-ante environmental assessments of novel technologies–Improved caprolactam catalysis and hydrogen storage. Journal of Cleaner Production. 19(14): 1659-1667.

Shu, Y.C. 2023. Research on fire and explosion risk assessment methods for LNG ship liquid cargo leakage accidents. Jiangsu University of Science and Technology.

Tanaka, T., Azuma, T., Evans, J.A., et al. 2007. Experimental study on hydrogen explosions in a full-scale hydrogen filling station model. International Journal of Hydrogen Energy. 32(13): 2162-2170.

Wang, Y., Xu, C., Zhao, G., et al. 2025. Numerical simulation study on hydrogen leakage and explosion of hydrogen fuel cell buses. Scientific Reports. 15(1): 319.

Xiao, H., Duan, Q., Sun, J. 2018. Premixed flame propagation in hydrogen explosions. Renewable and Sustainable Energy Reviews. 81: 1988-2001.

Xu, C.Y., Zhao, G.X., He, F.C. 2024. Numerical simulation analysis of hydrogen leakage and diffusion from hydrogen energy buses under environmental wind. Automobile Applied Technology. 49(02): 12-16.

Yang, F., Wang, T., Deng, X., et al. 2021. Review on hydrogen safety issues: Incident statistics, hydrogen diffusion, and detonation process. International Journal of Hydrogen Energy. 46(61): 31467-31488.

Zhao, M.B. 2021. Safety analysis of fuel cell vehicle leakage and explosion accidents in underground parking lots. Shandong University.

Vyazmina, E., Jallais, S. 2016. Validation and recommendations for FLACS CFD and engineering approaches to model hydrogen vented explosions: Effects of concentration, obstruction vent area and ignition position. International Journal of Hydrogen Energy. 41(33): 15101-15109.

Jie Chen is a lecturer at Henan Polytechnic University, mainly engaged in new energy security prevention and control and smart fire protection.